Journal of Inflammation Research

Dovepress
Taylor & Francis Group

Open Access Full Text Article

ORIGINAL RESEARCH

Astragaloside IV Attenuates Chronic Prostatitis by Activating Keap1/Nrf2/HO-1 Pathway: Suppressing Ferroptosis and Enhancing Antioxidant Defense

Jintao Shi[1,*], Yang Xuan[1–3,*], Qinyu Zhang[1,*], Jiangtao Chen[1], Weihan Zhu[1], Hao Zhang[2,3], Yue Duan[2,3]

[1]The Second Clinical Medical College, Zhejiang Chinese Medical University, Hangzhou, Zhejiang, 310053, People's Republic of China; [2]Department of Urology and Andrology, The Second Affiliated Hospital of Zhejiang Chinese Medical University, Hangzhou, Zhejiang, 310005, People's Republic of China; [3]Zhejiang Provincial Key Laboratory of Sexual Function of Integrated Traditional Chinese and Western Medicine, Hangzhou, Zhejiang, 310005, People's Republic of China

*These authors contributed equally to this work

Correspondence: Yue Duan; Hao Zhang, The Second Affiliated Hospital of Zhejiang Chinese Medical University, Xinhua Hospital of Zhejiang Province, No. 318, Chaowang Road, Hangzhou City, Zhejiang Province, People's Republic of China, Email dyurology@163.com; htjtcm@163.com

Background: Chronic prostatitis/chronic pelvic pain syndrome (CP/CPPS), a chronic inflammatory disorder with complex etiology and limited treatment options, is closely associated with oxidative stress and regulates cell death. Ferroptosis—an iron-dependent cell death driven by lipid peroxidation—amplifies CP/CPPS inflammation by concurrently triggering mitochondrial apoptosis and NLRP3 inflammasome activation, while Keap1/Nrf2/HO-1 axis serves as a central regulator bridging ferroptotic, apoptotic, and inflammatory cell death pathways. Astragaloside IV (AS-IV), a primary bioactive component of Astragalus membranaceus with established clinical use in urological therapies and favorable pharmacokinetics, was prioritized over structural analogs due to its unique dual-phase modulation: enhancing Nrf2 nuclear translocation without suppressing NF-κB-mediated immune surveillance. However, regulatory mechanisms linking AS-IV to ferroptosis inhibition in CP/CPPS remain unknown.

Patients and Methods: This study aimed to investigate the therapeutic potential of astragaloside IV (the primary bioactive component of *Astragalus membranaceus*) for the treatment of CP/CPPS by suppressing ferroptosis via the Keap1/Nrf2/HO-1 pathway. A rat CP/CPPS model was established using complete Freund's adjuvant (CFA), with animals divided into normal control, EAP, and AS-IV high/medium/low-dose groups and treated daily for four weeks. Additionally, a human prostatic epithelial cell (RWPE-1) inflammation model was induced by lipopolysaccharide (LPS), and cells were categorized into control, LPS, AS-IV medium-dose, ferroptosis inhibitor, and Nrf2 inhibitor + AS-IV medium-dose groups.

Results: AS-IV ameliorated prostatic tissue inflammation and fibrosis, reduced lipid peroxidation marker malondialdehyde (MDA) levels, and enhanced antioxidant indicators, including glutathione (GSH) content and glutathione peroxidase 4 (GPX4) activity. Western blotting and immunohistochemical analyses further confirmed that AS-IV activated the antioxidant pathway by suppressing Keap1 expression, promoting Nrf2 nuclear translocation, and upregulating heme oxygenase-1 (HO-1) protein levels. Concurrently, pro-inflammatory cytokine levels, including tumor necrosis factor-alpha (TNF-α) and interleukin-6 (IL-6), were markedly reduced.

Conclusion: This is the first study to demonstrate that AS-IV alleviates type III CP pathological damage by inhibiting ferroptosis via the Keap1/Nrf2/HO-1 axis, thereby providing experimental evidence for the development of multi-target therapeutic strategies based on natural products.

Keywords: prostatic inflammation, lipid peroxidation, Nrf2, cellular redox balance, oxidative stress, pharmacological activation

Received: 9 April 2025
Accepted: 16 July 2025
Published: 29 July 2025

Introduction

Chronic prostatitis/chronic pelvic pain syndrome (CP/CPPS) is a prevalent urological disorder affecting men worldwide, with epidemiological studies indicating a lifetime prevalence rate exceeding 50%. However, existing pharmacotherapies (including antibiotics and alpha-blockers) have demonstrated limited efficacy in approximately 46% of cases.[1–3] The condition is clinically characterized by persistent pelvic pain and lower urinary tract dysfunction; pathological mechanisms involve a complex interplay between oxidative stress, neuroinflammation, immune dysregulation, and tissue fibrosis.[4–6] Notably, ferroptosis, an iron-dependent, lipid peroxidation-driven form of non-apoptotic cell death, has been mechanistically linked to chronic inflammatory disorders. Emerging evidence suggests that this association may involve damage-associated molecular pattern (DAMP)-mediated activation of innate immunity, whereas cytokine storms within inflammatory microenvironments potentially disrupt lipid redox homeostasis. This creates a self-perpetuating pathological cycle in which oxidative stress triggers ferroptosis, which in turn exacerbates inflammation, potentially explaining the chronic progression of CP/CPPS.[6–8] In this context, the Keap1/Nrf2/HO-1 signaling pathway has garnered significant attention for its role in counteracting ferroptosis through modulation of antioxidant enzymes, including GPX4 and SOD. However, the mechanistic details of this pathway in CP/CPPS pathogenesis remain unclear. While the current understanding establishes that Keap1 regulates Nrf2 stability via ubiquitination-mediated degradation and that nuclear translocation of Nrf2 enables transcriptional activation of downstream targets such as HO-1 through binding to antioxidant response elements (ARE), the spatiotemporal regulatory dynamics of this signaling cascade within CP/CPPS microenvironments require further elucidation.[7,9,10]

From the perspective of traditional medicine, *Astragalus membranaceus* (Huang qi), documented in *Compendium of Materia Medica* for its effects in "enhancing qi circulation, activating blood flow, and promoting tissue regeneration" demonstrates pharmacological correlations with its modern pharmacologically identified active compound astragaloside IV (AS-IV). This tetracyclic triterpenoid saponin (C41H68O14) exhibits marked anti-inflammatory, antioxidant, and anti-fibrotic properties.[11–13] Current evidence indicates that AS-IV not only alleviates inflammatory responses in prostatic hyperplasia models through TLR4/NF-κB pathway inhibition, but also mitigates tissue fibrosis progression via MAPK signaling modulation.[14–16] Mechanistic investigations further reveal AS-IV's capacity to counteract oxidative stress-induced mitochondrial dysfunction, as evidenced by reduced lipid peroxidation biomarkers (MDA and ROS) and enhanced antioxidant enzyme activities (SOD and CAT).[14,17–19] Notably, while AS-IV has demonstrated ferroptosis-inhibitory effects in renal tubular epithelial cells through Nrf2 pathway activation, its precise regulatory mechanisms targeting the Keap1/Nrf2/HO-1 axis in CP/CPPS models remain unexplored.[20]

While the multi-target pharmacological activity of AS-IV offers novel therapeutic potential for CP/CPPS, three critical gaps remain: (1) The spatiotemporal activation patterns of ferroptosis in prostatic tissues and their causal relationship with pain/fibrosis phenotypes require systematic validation, with limited evidence demonstrating disease improvement through ferroptosis inhibition; (2) The Keap1/Nrf2/HO-1 pathway exhibits dual regulatory effects on ferroptosis, where HO-1 demonstrates both cytoprotective antioxidant functions and paradoxical pro-ferroptotic activity via heme degradation-derived iron liberation, necessitating further investigation into its homeostatic regulation within the CP/CPPS microenvironment; (3) Despite established anti-inflammatory/antioxidant properties of AS-IV, its potential to disrupt the "inflammation-ferroptosis" cycle through Keap1/Nrf2/HO-1-mediated ferroptosis suppression in prostate cells remains unexplored.[21–23] Current monotherapeutic approaches for CP/CPPS demonstrate limited efficacy, underscoring the clinical need for multi-target interventions leveraging natural product derivatives.

Building upon this foundation, our study investigates ferroptosis as a pathological driver in CP/CPPS progression and elucidates the therapeutic mechanism of AS-IV through Keap1/Nrf2/HO-1 signaling.[6] Three objectives guide this research: (1) Establish temporal correlations between ferroptosis markers (GPX4, ACSL4, lipid ROS), inflammatory mediators (IL-6, TNF-α), and fibrotic progression (collagen deposition, TGF-β1) through longitudinal monitoring in CP/CPPS rat models; (2) Decipher AS-IV's molecular regulation of Nrf2 nuclear translocation and subsequent HO-1/GPX4 upregulation through integrated approaches: Molecular docking and co-immunoprecipitation (Co-IP) analyses Nrf2 conditional knockout models Functional validation of iron homeostasis and glutathione system modulation; (3) Determine AS-IV's ferroptosis-dependent therapeutic effects through pharmacological challenges using Ferroptosis

inducer Erastin HO-1 inhibitor zinc protoporphyrin (ZnPP) to establish the "AS-IV → Keap1/Nrf2/HO-1 → ferroptosis suppression" mechanistic cascade.

This study pioneered the integration of ferroptosis mechanisms with the active components of traditional Chinese medicine (TCM), establishing a novel research direction for understanding the pathogenesis and developing therapeutic strategies for CP/CPPS. Theoretically, this study elucidates the "oxidative stress-ferroptosis-chronic inflammation" axis and reveals the dual regulatory mechanisms of the Keap1/Nrf2/HO-1 signaling pathway, significantly advancing our understanding of programmed cell death in chronic inflammatory diseases. By combining ferroptosis mechanisms with the multi-target characteristics of TCM, this research proposes a novel paradigm: If experimental validation confirms AS-IV can stabilize Nrf2 to inhibit HO-1-mediated ferroptosis, it will establish a "dual regulatory balance" model for natural compounds in modulating cell death pathways. Practically, the identified multi-target therapeutic effects of AS-IV on ferroptosis regulation not only offer a safe adjuvant therapy for CP/CPPS, but also establish a "multi-effect drug" development framework for natural compounds, demonstrating significant translational potential.[20] Furthermore, the identified molecular targets of AS-IV (Nrf2, GPX4) show broad applicability in ferroptosis-associated pathologies including renal fibrosis and neurodegenerative diseases, indicating extensive scientific value and clinical translation prospects.

Materials and Methods

Animals

Adult male Sprague-Dawley rats (weight range 250–350 g) were obtained from Shanghai Sippr-BK Laboratory Animal Co., Ltd. (Certification No. SCXK [Hu] 2023–0009). Animals were housed at the Laboratory Animal Research Center of Zhejiang Chinese Medical University (certification no. SYXK [Zhe] 2021–0012) under standardized conditions: ambient temperature 20–24°C, relative humidity, 50 ± 5%, 12-hour light/dark cycle, with ad libitum access to food and water. All the experimental protocols were approved by the Ethics Committee of Zhejiang Chinese Medical University (approval no. IACUC-20221024-05), and was conducted in accordance with the National Institutes of Health Guide for the Care and Use of Laboratory Animals.

Reagents

Reagents and antibodies were sourced as follows: Complete Freund's Adjuvant (CFA) from Sigma-Aldrich (St. Louis, MO, USA); Astragaloside IV (CAS 84687–43-4) from Macklin (Shanghai, China); ML385 (HY-100523), Ferrostatin-1 (HY-100579), and Erastin (HY-15763) from MedChemExpress (Monmouth Junction, NJ, USA). Oxidative stress assay kits, including those for malondialdehyde (MDA, S0131S), Superoxide Dismutase (SOD, S0101S), Lactate Dehydrogenase Cytotoxicity (C0018S), glutathione (GSH/GSSG, S0053), CCK-8 (C0039), and Reactive Oxygen Species (S0033S) were obtained from Beyotime Biotechnology (Shanghai, China). The cellular ferrous colorimetric assay kit (E-BC-K881-M) was obtained from Elabscience (Wuhan, China), Lipopolysaccharides (L2880) from Sigma (Shanghai, China), and human normal prostate epithelial cells (STM-CL-5405) from ScienCell (Shanghai, China). Primary antibodies against Anti-Nrf2 (#12721), Anti-Keap1 (#8047), Anti-xCT (#98051), Anti-GPX4 (#52455), Anti-GAPDH (#2118), and Anti-β-actin (#4970) were purchased from Cell Signaling Technology (Danvers, MA, USA). Anti-HO-1 (10701-1-AP), Anti-FTH1 (83428-1-RR), and Anti-TNF-α (83721-7-RR) were purchased from Proteintech (Rosemont, IL, USA). Secondary antibody: HRP-conjugated goat Anti-mouse (RGAM001) from Proteintech.

Animal Treatment

An experimental autoimmune prostatitis (EAP) rat model was established as previously described.[24,25] Briefly, prostate tissues were harvested from euthanized adult male Sprague-Dawley rats, homogenized in PBS, and centrifuged at 12,000 ×g for 15 min to obtain prostate antigen (PAg)-containing supernatant. PAg (300 μg/rat) or PBS control was emulsified with Complete Freund's Adjuvant (CFA) at 1:1 ratio. The EAP and treatment groups received subcutaneous injections of the CFA-PAg emulsion (1 mL total volume distributed at four sites: bilateral hind footpads, dorsum, and tail base), whereas the control group received the CFA-PBS emulsion. Immunization was performed twice (days 0 and 28) to

establish a chronic EAP. From day 28 post-boost, the treatment groups received AS-IV daily via oral gavage for 15 days, prior to sacrifice on day 42. AS-IV was dissolved 10% DMSO + 90% (20% SBE-β-CD in saline) and administered at three dose levels: 10, 20, 40 mg/kg/day (n=6/group).[26] Experimental groups included: (1) Normal control (PBS + vehicle), (2) EAP model (PAg+vehicle), (3) EAP+AS-IV-Low, (4) EAP+AS-IV-Mid, (5) EAP+AS-IV-High.[13] All control groups received vehicle-matched solution (10% DMSO + 90% 20% SBE-β-CD/saline) via identical gavage procedures to ensure operational parity.

Histological Evaluation

Following 24-hour fixation in 4% paraformaldehyde (pH 7.4) at room temperature, prostate tissues were subjected to standard histological processing, including gradient ethanol dehydration, xylene clearing, and paraffin embedding. Serial 4-μm sections were prepared using a rotary microtome (RM2235, Leica). Hematoxylin (Cat#G1005, Servicebio) and eosin (H&E) staining was performed using standard protocols. Whole-slide scanning was performed using a Nikon Eclipse Ti inverted microscope equipped with a DS-Ri2 camera. Quantitative analysis was performed using ImageJ 1.53t (NIH) with a color deconvolution plugin for stain separation. Blinded histopathological evaluation was performed by two independent pathologists: 1. Acinar structural disorganization, 2. basal cell layer integrity and 3. Stromal inflammatory cell density; 4. perivascular cuffing severity, and 5. Extent of focal hemorrhage A modified 5-tier semi-quantitative scoring system was applied: 0, normal architecture;1, focal alterations (<25% field);2, regional involvement (25–50%);3, extensive changes (50–75%); and 4, diffuse pathology (>75%).[27]

Cell Lines and Culture

Normal human prostate epithelial cells (RWPE-1, STM-CL-0216, ScienCell, Shanghai, China) were maintained in a water-jacketed CO_2 incubator (Forma Series II, Thermo Scientific) at 37°C, 5% CO_2, and 95% humidity. The cells were cultured in RPMI-1640 complete medium (Cat# 31800022, Gibco) supplemented with 10% fetal bovine serum (FBS; Cat# 10270106, Gibco), 1% penicillin-streptomycin (Cat# 15140122, Gibco), and 2 mM L-glutamine (Cat# 25030081, Gibco).

Subculturing was performed when the cells reached 80–90% confluence. Briefly, the culture medium was aspirated and the cells were washed twice with Dulbecco's phosphate-buffered saline (DPBS, Cat# 14190144, Gibco). Enzymatic dissociation was achieved using 0.25% trypsin-EDTA solution (Cat# 25200072, Gibco) for 3 min at 37°C. The enzymatic reaction was neutralized using a complete medium. The cells were centrifuged at 300 ×g for 5 min (Eppendorf 5810R), resuspended in fresh medium, and seeded at 1:3–1:4 split ratios. All experiments used cells between passages 3–8, with viability >95%, as determined by the trypan blue exclusion assay.

Cell Viability Assay

RWPE-1 cells in the logarithmic growth phase (passages 3–5) were seeded into 96-well plates at 5×10^3 cells/well density. Six technical replicates were arranged in PBS-filled perimeter wells to minimize edge effects. After 12-hour adherence, treatments were administered: Control: Complete RPMI-1640 medium; LPS, 1 μg/mL LPS for 24 h (inflammatory model induction); Ast-M, LPS priming followed by 20 μM AS-IV for 24 hr7; Fe+, LPS + 200 μM Ferrostatin-1 (ferroptosis inhibitor)7; Nrf2-, LPS + 20 μM;Astragaloside IV + 5 μM ML385 (Nrf2 inhibitor). Cell viability was assessed using the CCK-8 kit; after removing the medium, 10 μL CCK-8 reagent mixed with 90 μL serum-free medium was added per well, followed by a 2-hour incubation at 37°C in the dark. Absorbance was measured at 450 nm (reference: 650 nm) using a SpectraMax i3x microplate reader (Molecular Devices). Data analysis was performed using GraphPad Prism 9.0 using one-way ANOVA with Tukey's post-hoc test.[28]

Detection of Intracellular ROS Levels

RWPE-1 cells were seeded on sterile coverslips in 6-well plates at 5×10^4 cells/well. The experimental groups were subjected to the CCK-8 assay. After treatment, the cells were subjected to ROS detection at 1. Probe Loading: Washed three times with pre-warmed PBS (37°C); 2. Cells were incubated with 10 μM 2′,7′-dichlorodihydrofluorescein diacetate (DCFH-DA) in serum-free medium at 37°C for 20 min (protected from light). After probe removal, cells were fixed with

4% paraformaldehyde for 15 min at RT. The coverslips were mounted using an antifade medium and imaged using a Nikon Eclipse Ti microscope (FITC channel, Ex/Em=488/525 nm).

Estimation of Oxidative Stress

Superoxide dismutase (SOD) serves as a key enzymatic antioxidant for free radical scavenging, SOD activity reflects superoxide anion (O_2^-) scavenging capacity, measured by the inhibition rate of WST-8 formazan formation at 450 nm, while malondialdehyde (MDA) is a lipid peroxidation marker reflecting both membrane damage and oxidative stress intensity.[29] Blood samples were collected via retro-orbital bleeding into coagulation-activated tubes. After 30-min of clotting at room temperature, serum was separated by centrifugation at 2,000 ×g for 15 min at 4°C. Serum SOD activity and MDA content were measured using commercial kits (Beyotime, China), according to the manufacturer's protocol. Final values were normalized to the total protein concentration determined using the BCA assay.

Immunohistochemistry

Prostate paraffin sections (4 μm) were subjected to xylene gradient dewaxing and ethanol series rehydration. Heat-induced epitope retrieval (HIER) was performed in citrate buffer (pH 6.0; 10 mM sodium citrate, 0.05% Tween 20) at 95° C for 20 min, using a histoprocessor (PT Module, Thermo Scientific). Endogenous peroxidase activity was quenched using 3% H_2O_2 in methanol (Cat# P0101A; Beyotime Biotechnology, Shanghai, China) for 15 min at RT. Non-specific binding was blocked with 5% normal goat serum (Cat# C0265, Beyotime) for 1 h at 37°C in a humidified chamber. The sections were incubated with an anti-Nrf2 primary antibody (1:100 dilution, Cat# ab137550, Abcam, Cambridge, UK) at 4°C overnight. Following PBS-T washes, HRP-conjugated secondary antibody (Cat# GB23303, 1:500, Servicebio, Wuhan, China) was applied for 1 hr at 37°C. DAB chromogen (Cat# K3468, DAKO, Glostrup, Denmark) was developed by microscopic monitoring (3–5 min). Hematoxylin counterstaining (Gill's formulation) was optimized using acid-alcohol differentiation (1% HCl in 70% ethanol). Following blueing in Scott's tap water substitute, the sections were dehydrated using graded alcohols, cleared in xylene, and mounted with Permount (SP15-500, Fisher Scientific). Digital imaging was performed using a Nikon Eclipse 80i microscope equipped with a DS-Fi2 camera.

Immunofluorescence Assay

Immunofluorescence (IF) was performed to assess the subcellular localization of the proteins. RWPE-1 cells (1×10^4/well) on coverslips were treated as per CCK-8 experimental groups. After treatment, the cells were fixed with 4% paraformaldehyde (15 min at RT) and permeabilized with 0.25% Triton X-100 (3 min at RT). Nonspecific binding was blocked with 1% BSA (A8020, Solarbio) in PBS for 30 min at RT. For tissue IF: Paraffin sections (5 μm) were subjected to antigen retrieval in EDTA buffer (pH 8.0, Cat# C1031, Beyotime) using microwave irradiation (800 W for 5 min and 400 W for 15 min). The sections were permeabilized with 0.3% Triton X-100 (T9284, Sigma) for 15 min and blocked with 5% donkey serum (017–000-121, Jackson) for 1 h. Primary antibody incubation: Tissue: Anti-Nrf2 (1:200, ab137550, Abcam) for 16 h at 4°C; Cell mono-staining: Anti-Nrf2/Keap1/GPX4/HO-1 (1:200, CST/Proteintech); Cell dual-staining: 1st cycle: rabbit anti-Keap1 (1:100, 8047S, CST) for 16 h at 4°C,2nd cycle: mouse anti-Nrf2 (1:200, ab89443, Abcam) after cross-blocking with 10% donkey serum. Secondary detection CoraLite 488-conjugated antibodies (1:500, SA00013-2, Proteintech) were incubated for 1 h at 37°C in the dark. The nuclei were counterstained with DAPI (D9542, Sigma) for 5 min and then mounted with ProLong Diamond (P36961, Thermo Fisher). Images were acquired using a Nikon A1R confocal microscope equipped with a 60× oil objective lens.

LDH Release Assay

Fresh prostate tissues (100 mg) were homogenized in 1 mL ice-cold assay buffer (Cat# C0017, Beyotime) using a tissue homogenizer (T10 basic, IKA) with three 30-second pulses at 15,000 rpm and interspersed at ice-cooling intervals. Following homogenization, lysates were centrifuged at 12,000 ×g for 15 min at 4°C. The supernatant was collected for measuring LDH activity using a WST-8-based LDH Cytotoxicity Assay Kit (Cat# C0019S, Beyotime) as follows: 1. Working solution preparation: Mix the enzyme solution and chromogenic substrate at a 1:45 (v/v) ratio, 2. Reaction setup: 50 μL of sample was combined with 50 μL of working solution in a 96-well plate, 3. Incubation: Protect from light

and incubate at 37°C for precisely 30 min; 4. Detection: Absorbance was measured at 450 nm using a microplate reader with a 650 nm reference filter.

Glutathione Level Assay

Total and oxidized glutathione levels in prostate homogenates and cell lysates were quantified in triplicate using the Glutathione Assay Kit (Cat# S0053, Beyotime). The results were normalized to the total protein concentration determined by bicinchoninic acid (BCA) assay (Cat# P0012, Beyotime), expressed as nmol GSH/mg protein.

Western Blotting Assay

Rat prostate tissues were homogenized in pre-chilled grinding tubes containing RIPA lysis buffer (50 mM Tris-HCl pH 7.4, 150 mM NaCl, and 1% NP-40) supplemented with a protease/phosphatase inhibitor cocktail (Cat# P0013B, Beyotime) at a 1:10 (w/v) ratio using a mechanical homogenizer (IKA T10, Germany). For protein extraction, RWPE-1 cells were washed with PBS and lysed in ice-cold RIPA buffer. Lysates were centrifuged at 12,000 ×g (4°C, 15 min) and the supernatants were quantified using the Pierce™ BCA Protein Assay Kit (Cat# 23227, Thermo Fisher). Protein samples (20 μg) were mixed with 5× Laemmli buffer containing 2% β-mercaptoethanol and denatured at 100°C for 10 min in a digital dry bath. SDS-PAGE was performed using Mini-PROTEAN Tetra System (Bio-Rad): 10% separating gel (120 V constant voltage for 90 min) and 5% stacking gel (80 V until dye front entered separating gel). Proteins were transferred to 0.45 μm PVDF membranes (IPFL00010, Millipore) via wet transfer (300 mA, 40 min) in Tris-glycine buffer containing 20% methanol. Membranes were blocked with 5% non-fat milk in TBST (50 mM Tris, 150 mM NaCl, 0.1% Tween 20, pH 7.6) for 2 h at RT. Primary antibodies diluted in blocking buffer were applied overnight at 4°C: KEAP1 (1:1000, #8047, CST), Nrf2 (1:1000, #12721, CST), HO-1 (1:2000, 10701-1-AP, Proteintech), GPX4 (1:1000, #52455, CST), FTH1 (1:2000, 83428-1-RR, Proteintech), xCT/SLC7A11 (1:1000, #98051, CST), TNF-α (1:1000, 83721-7-RR, Proteintech), GAPDH (1:5000, #2118, CST), β-actin (1:5000, #4970, CST). After three TBST washes (10 min each), the membranes were incubated with an HRP-conjugated goat anti-mouse/rabbit secondary antibody (1:5000, RGAM001, Proteintech) for 1 h at RT. Signal development was performed using ECL Plus Substrate (Cat# 35055, Thermo Fisher). Protein bands were captured using the ChemiDoc MP Imaging System (Bio-Rad) and quantified using the Image Lab 6.1 software. The relative expression levels were normalized to those of β-actin and GAPDH.

RT-qPCR

RWPE-1 cells (5×10^5/well) were lysed after 48-hour treatment. Total RNA was isolated from cells and rat prostate tissues using the Steadypure RNA Extraction Kit (AG11728, Accurate Biology, Changsha, China). RNA purity (A260/A280=1.8–2.1) and concentration were verified using a NanoDrop 2000 (Thermo Scientific). Reverse transcription was performed with 1 μg of RNA using HiScript III RT SuperMix (R323-01, Vazyme, Nanjing, China) under the following thermal conditions: 42°C for 15 min, followed by 85°C for 5 s. qPCR amplification was performed using SYBR Green Pro Taq HS Premix (DBI-2213; DBI Bioscience, Shanghai, China) on a QuantStudio 6 Pro System (Thermo Fisher Scientific). Reaction mixture (20 μL): 10 μL 2× Master Mix, 0.8 μL each primer (10 μM), 2 μL cDNA template, 7.2 μL nuclease-free water. Thermal profile: 95°C for 30s (initial denaturation); 40 cycles of 95°C for 5s and 60°C for 30s; melt curve analysis (60–95°C, 0.3°C/s). Primers (Table 1) were designed using NCBI Primer-BLAST with amplicons spanning exon-exon junctions (80–150 bp). Relative quantification was performed using the ΔΔCt method with three biological replicates.

Molecular Docking

Structures of the active ingredient compounds were downloaded from the PubChem database, and the three-dimensional crystal structure of the target protein was downloaded from the PDB database. Sitemap was used for the active-site prediction. It was processed using the Schrödinger's Protein Preparation module, including residue repair, hydrogen bond optimization, solvent removal, and energy minimization. The ligand was prepared using the LigPrep module with an OPLS3e force field, ionized, and minimized. The preprocessed protein and ligand were then docked using the Ligand

Table 1 RT-qPCR Primer Sequence

Gene	Primer	Sequence (5′–3′)	PCR Products (bp)
β-actin	Forward	TGGCACCCAGCACAATGAA	161
	Reverse	CTAAGTCATAGTCCGCCTAGAAGCA	
Mus Keap1	Forward	TGCATCCACCACAACAGTGT	156
	Reverse	ATTAAGGCGGTTTGTCCCGT	
Mus Nrf2	Forward	GTATGCAACAGGACATTGAGCAAG	107
	Reverse	TGGAACCATGGTAGTCTCAACCAG	
Mus GPX4	Forward	CAGTGAGGCAAGACCGAAGTA	103
	Reverse	CGAACTGGTTACACGGGAAGG	
Mus HO-1	Forward	GGAACTTTCAGAAGGGCCAGGT	148
	Reverse	TGCAGCTCTTCTGGGAAGTAGACA	

Docking module, selecting the prepared Grid and Lig files, and using the Glide module for standard precision docking. After clicking "Run" the docking results were obtained. Finally, the results were visualized using PyMol software.

Data and Statistical Analysis

Statistical analyses were performed using GraphPad Prism 9.0 (GraphPad Software, San Diego, CA, USA). Data normality was assessed using the Shapiro–Wilk test. Parametric data were analyzed using One-way ANOVA with Tukey's post hoc test (multiple group comparisons) and Two-way ANOVA with Sidak's correction (two factorial designs), and non-parametric data were evaluated using the Kruskal–Wallis test with Dunn's post hoc analysis. All measurements are presented as mean ± standard deviation (SD). Statistical significance thresholds: $*P < 0.05$, $**P < 0.01$, $***P < 0.001$, $****P < 0.0001$.

Results

Astragaloside IV Attenuates Prostatic Inflammation in Experimental Autoimmune Prostatitis (EAP) Rats

Following the successful establishment of the EAP rat model (Figure 1A), the therapeutic effects of AS-IV were dose-dependently evaluated.[30] H&E staining revealed substantial inflammatory infiltration in the EAP group prostates, which was progressively attenuated with AS-IV treatment (Figure 1B and C). Semi-quantitative histopathological scoring demonstrated a significant reduction in the inflammation scores (Figure 1C and D).[31] These findings confirm the anti-inflammatory efficacy of AS-IV in EAP pathophysiology.

Astragaloside IV Treatment Activates Nrf2 Signaling in Ferroptosis Pathways Through Multi-Level Molecular Regulation

In this study, we investigated the effects of AS-IV on Nrf2 activation by Western blotting (Figures 2A–E). The experimental groups included control, EAP (untreated disease group), and low-, medium-, and high-dose AS-IV treatment. The EAP group exhibited significant inflammatory responses after disease induction, suggesting activation of the ferroptosis pathway. AS-IV treatment markedly increased Nrf2 protein levels, particularly in the medium- and high-dose groups, with expression significantly surpassing that in the EAP group (Figure 2D). Interestingly, we observed a simultaneous increase in KEAP1 and Nrf2 expression, which contradicts the established understanding that KEAP1 typically suppresses Nrf1. Potential explanations include the following: 1. AS-IV may activate Nrf2 through non-classical pathways (eg as PI3K/AKT signaling), while upregulating KEAP1 as a compensatory feedback mechanism.

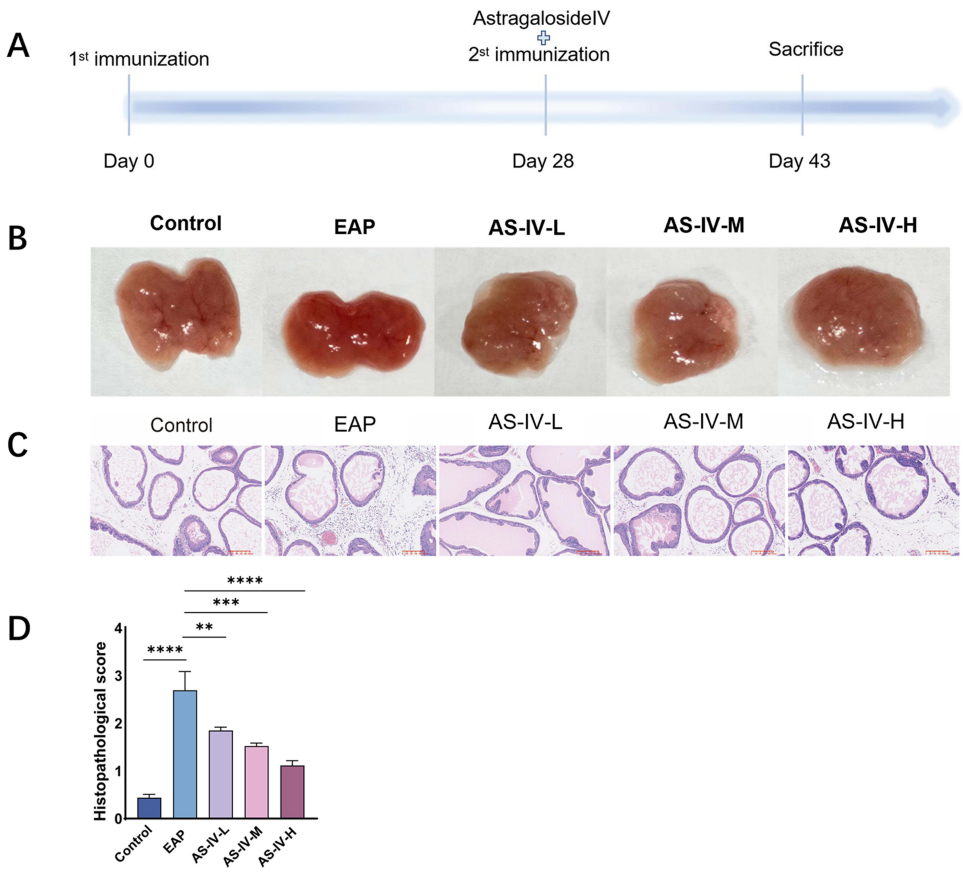

Figure 1 Astragaloside IV treatment alleviates EAP-associated prostatitis. (**A**) Schematic of the experimental protocol for Astragaloside IV administration in EAP rat models. (**B**) Representative prostate tissue sections from control, EAP model, and Astragaloside IV-treated groups. (**C**) Hematoxylin and eosin (H&E) staining showed that the infiltrating inflammatory cells in prostate tissues was significantly reduced in EAP rat after AS-VI treatment. (**D**) Histopathological scoring comparison between EAP model and AS-IV treatment groups. Data presented as mean ± SD. Statistical analysis performed using Kruskal–Wallis non-parametric test. Significance levels: ns (not significant) $P>0.05$; *$P<0.05$; **$P<0.01$; ***$P<0.001$; ****$P<0.0001$.

2. Accelerated degradation of the KEAP1-Nrf2 complex under pathological conditions may occur, with AS-IV restoring the cellular balance. Western blot analysis confirmed these findings; nuclear translocation of Nrf2 increased substantially in the AS-IV-treated groups, with KEAP1 expression showing a parallel upward trend, peaking in the medium-dose group (Figure 2D). To assess the cellular oxidative stress responses, we measured the levels of superoxide dismutase (SOD), glutathione (GSH), and lactate dehydrogenase (LDH) (Figure 2F, G and I). High-dose AS-IV treatment significantly elevated SOD activity and GSH concentration compared with those in the EAP group ($P < 0.01$), demonstrating potent antioxidant effects (Figure 2F and G).[32] LDH activity analysis revealed reduced cellular damage in the AS-IV-treated groups, with both the low- and medium-dose groups showing decreased LDH levels compared to the EAP group (Figure 2I). Furthermore, ferrous ion quantification revealed a significant reduction in iron accumulation after AS-IV treatment, which effectively suppressed ferroptosis (Figure 2H). Mechanistic studies have indicated that AS-IV enhances cellular antioxidant responses via the activation of the Nrf2/Keap1 pathway. Keap1 normally suppresses Nrf2 by binding to it, blocking its nuclear translocation and transcriptional activity.[33] However, reduced Keap1 expression allows Nrf2 to escape degradation, enter the nucleus, and upregulate antioxidant genes, including HO-1 and GPX4 (Figure 2B and E).[34] These antioxidant genes effectively reduced oxidative stress and suppressed lipid peroxidation, thereby inhibiting ferroptosis. To confirm Nrf2 regulation by AS-IV, we performed immunohistochemistry (IHC) and immunofluorescence (IF) of prostate tissues. Both IHC and IF analyses showed intensified Nrf2 staining in the treatment groups, particularly at medium and high doses, which was consistent with the Western blot results (Figure 2J and K). Furthermore, Nrf2 activation correlates with improved iron homeostasis, and this dual regulation of redox balance and iron metabolism underscores its antiferroptotic mechanism.

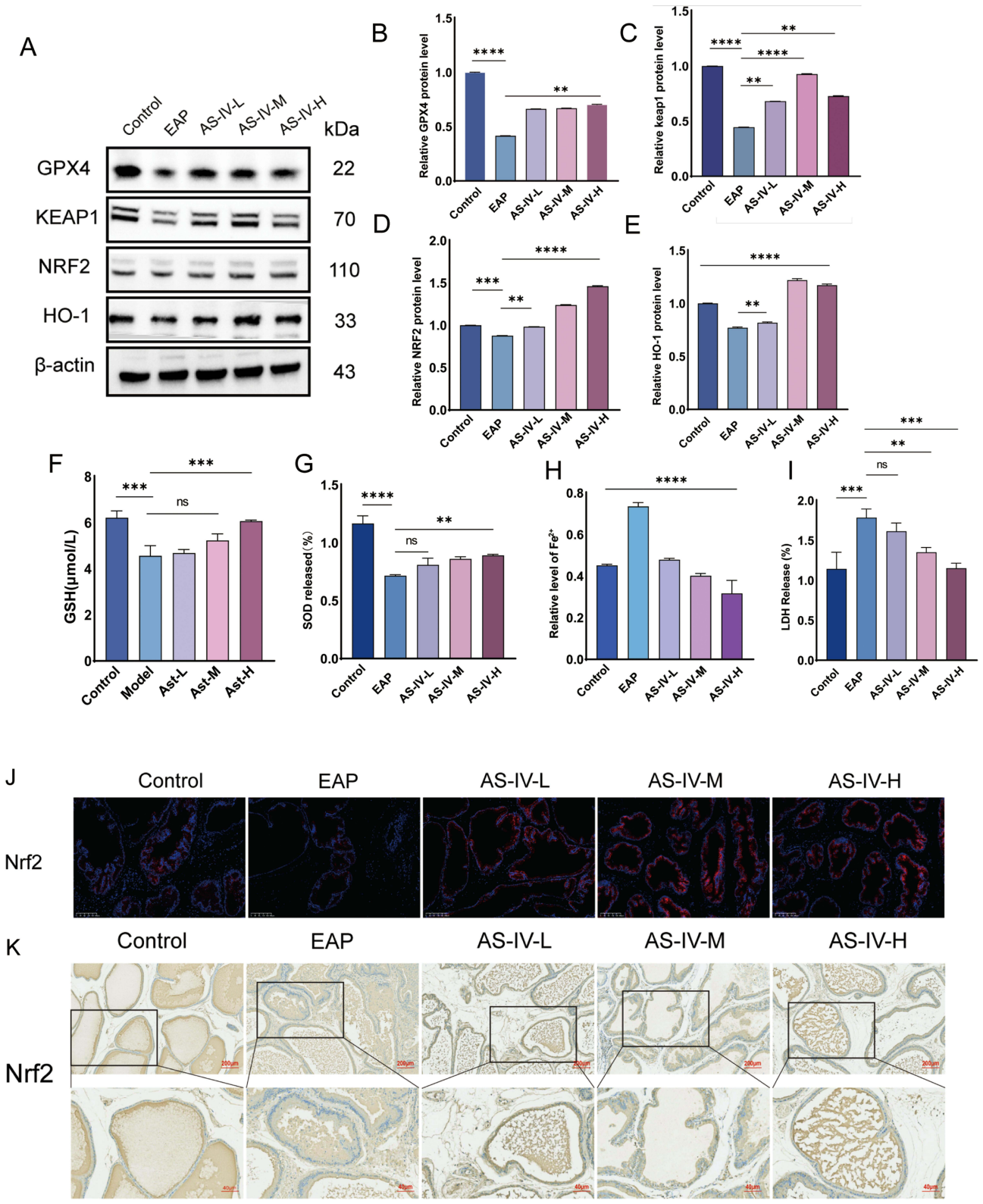

Figure 2 Astragaloside IV treatment enhanced Nrf2 nuclear translocation. (**A**) Western blot analysis of GPX4, Keap1, Nrf2, and HO-1 protein expression in prostate tissues from EAP model and AS-IV-treated rats. (**B**–**E**) Quantitative analysis of GPX4, Keap1, Nrf2, and HO-1 protein expression levels via Western blot. (**F**–**I**) Serum biomarkers analysis: Glutathione (GSH), superoxide dismutase (SOD), iron ion levels, and lactate dehydrogenase (LDH) activity. (**J** and **K**) Enhanced Nrf2 immunoreactivity demonstrated by immunohistochemical (IHC) and immunofluorescence (IF) staining in AS-IV-treated group. Data represent mean ± SD. Statistical significance determined by one-way ANOVA (**B**–**I**). Significance thresholds: ns (not significant) $P>0.05$; *$P<0.05$; **$P<0.01$; ***$P<0.001$; ****$P<0.0001$.

https://doi.org/10.2147/JIR.S527722

LPS-Induced Inflammatory Modeling in RWPE-1 Cells Promotes Ferroptosis Through Redox Imbalance and Iron Dysregulation

In the present study, we established an LPS-induced inflammatory model using RWPE-1 cells to investigate the molecular link between inflammation and ferroptosis. Western blot analysis demonstrated significant upregulation of TNF-α and IL-1 in LPS-treated cells compared to controls (Figure 3A–C). Notably, these inflammatory mediators exacerbate oxidative stress and modulate iron metabolism-related genes, thereby indirectly promoting ferroptosis. TNF-α suppresses ferroportin (FPN), (Ferritin Heavy Chain 1) FTH1 expression, leading to intracellular iron overload and Fenton reaction-driven ROS production (Figure 3D).[35] LPS treatment significantly reduced the SOD activity (Figure 3E) and depleted GSH levels (Figure 3F). Impaired SOD function disrupts superoxide anion (O_2^-) conversion to H_2O_2, whereas GSH deficiency compromises GPX4-mediated lipid peroxide reduction.[22] This dual defect amplifies hydroxyl radical (˙OH) generation via the Haber-Weiss reaction, causing irreversible oxidation of membrane phospholipids.[22]

Astragaloside IV Suppresses Ferroptosis and Alleviates Oxidative Stress in RWPE-1 Cells

To evaluate the protective effects of AS-IV against ferroptosis and oxidative stress in RWPE-1 cells, experimental groups were treated with control, LPS (untreated), and medium-dose AS-IV. The cell viability was assessed using the CCK-8 assay

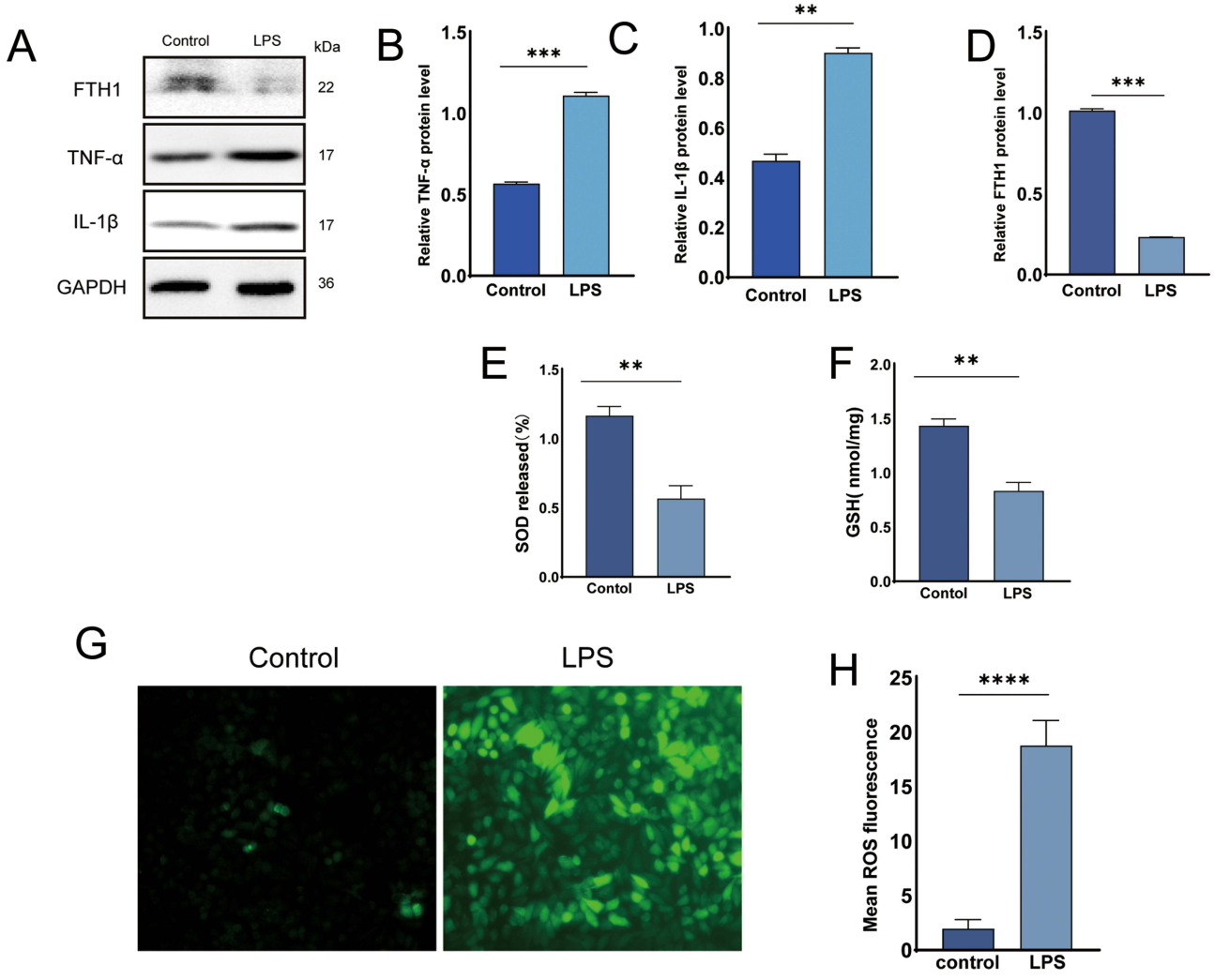

Figure 3 LPS induces inflammatory response and ferroptosis in RWPE-1 cells. (**A**) Western blot analysis of TNF-α, IL-1β and FTH1 expression in LPS-stimulated RWPE-1 cells with/without AS-IV treatment. (**B**–**D**) Quantitative analysis of FTH1, TNF-α, and IL-1β protein expression via Western blot. (**E** and **F**) Intracellular antioxidant capacity: Glutathione (GSH) levels and superoxide dismutase (SOD) activity. (**G**) Representative fluorescence images showing intracellular ROS accumulation. (**H**) Quantitative measurement of ROS fluorescence intensity. Data presented as mean ± SD. Statistical comparisons performed using one-way ANOVA (B-F, H). Significance designations: ns $P>0.05$; *$P<0.05$; **$P<0.01$; ***$P<0.001$; ****$P<0.0001$.

(Figure 4A). The LPS group showed significantly reduced survival compared to the control group, whereas AS-IV treatment restored cell viability, demonstrating cellular protection. Subsequent analysis of superoxide dismutase (SOD) activity and lactate dehydrogenase (LDH) release revealed elevated oxidative stress and membrane damage in the LPS group; SOD activity decreased by 58% and LDH release increased 2.3-fold compared to the control (Figure 4B and C). Medium-dose AS-IV treatment normalized these parameters: SOD activity recovered to 85% of the control levels, and LDH release was reduced by 64% (Figure 4 and C). Reactive oxygen species (ROS) quantification showed a 3.1-fold increase in the LPS group, which was reduced by 72% following AS-IV treatment, confirming its antioxidant capacity (Figure 4D). Furthermore, glutathione (GSH) analysis revealed significantly lower levels in the LPS group, which were restored by AS-IV treatment (Figure 4E).[36] This demonstrates its ability to enhance cellular antioxidant defense. Ferrous ion quantification revealed elevated iron accumulation in the LPS group that was markedly reduced by AS-IV treatment (Figure 4F), thereby confirming its role in the suppression of ferroptosis. Western blot analysis of the ferroptosis-related protein FTH1 demonstrated increased expression in the LPS group, which was significantly attenuated by AS-IV (Figure 4G and H). This suggests that AS-IV inhibits ferroptosis by downregulating FTH1 expression. In summary, AS-IV effectively prevents ferroptosis in RWPE-1 cells by mitigating oxidative stress (reduced ROS and enhanced SOD/GSH activity), decreasing membrane damage (lower LDH release), restoring iron homeostasis (reduced ferrous ions), and modulating FTH1 expression. These findings highlight its therapeutic potential in redox imbalance-related pathologies.

Astragaloside IV Prevents Ferroptosis in RWPE-1 Cells by Activating the Nrf2 Antioxidant Pathway

This study investigated the mechanism by which AS-IV suppresses ferroptosis in RWPE-1 cells through Nrf2 pathway activation, and evaluated its effects on oxidative stress. The experimental groups included the control, LPS (untreated), medium-dose AS-IV, ferroptosis inhibitor, and Nrf2 inhibitor + medium-dose AS-IV. CCK-8 assay revealed that medium-dose AS-IV significantly increased cell viability, indicating its role in promoting cell survival and inhibiting cell death (Figure 5A). LDH release analysis demonstrated reduced membrane damage, with AS-IV treatment lowering LDH levels by 64% compared to the LPS group ($P < 0.01$, Figure 5B). AS-IV restored glutathione (GSH) levels to 85% of the control values

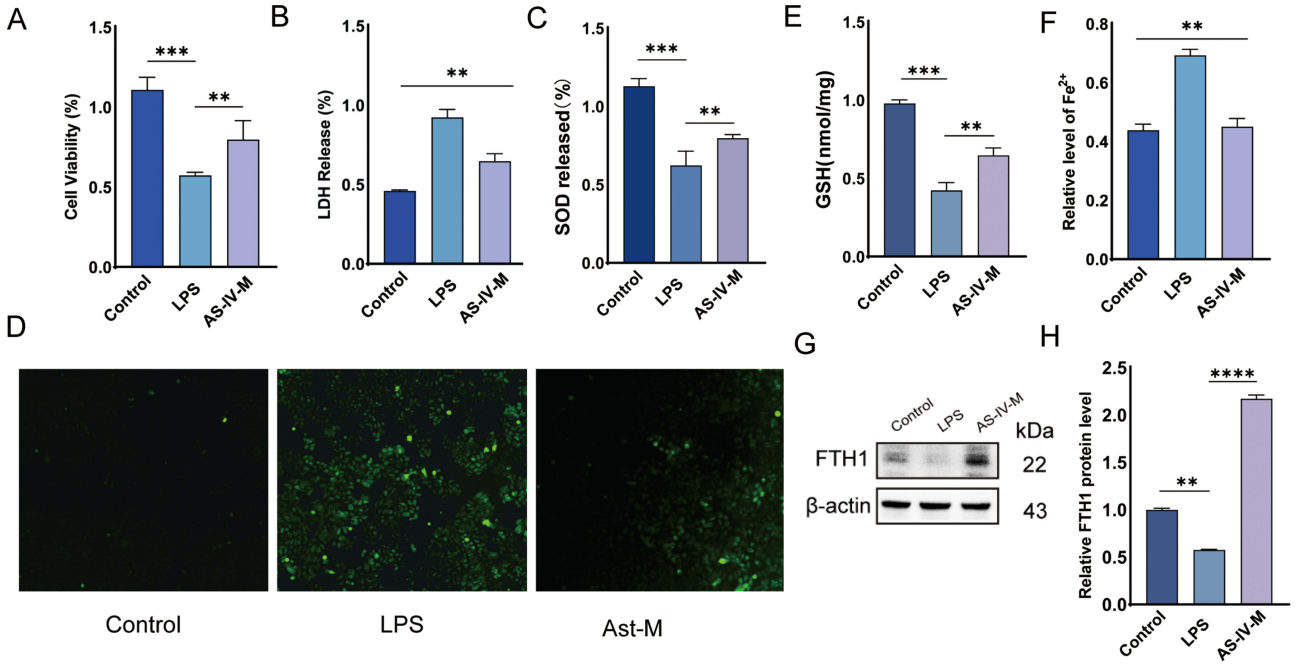

Figure 4 Astragaloside IV attenuates oxidative stress and inhibits ferroptosis in RWPE-1 cells. (**A**) Western blot analysis of ferritin heavy chain 1 (FTH1) expression in LPS-stimulated RWPE-1 cells with/without AS-IV treatment. (**B**) Quantitative analysis of FTH1 protein expression via Western blot. (**D**–**G**) Biochemical profiling showing lactate dehydrogenase (LDH) release, glutathione (GSH) content, superoxide dismutase (SOD) activity, and iron ion concentrations. (**H**) Intracellular ROS accumulation visualized through fluorescence microscopy. Data represent mean ± SD. Statistical significance determined by one-way ANOVA (**B**–**G**). Significance thresholds: ***P*<0.01; ****P*<0.001; *****P*<0.0001.

https://doi.org/10.2147/JIR.S527722

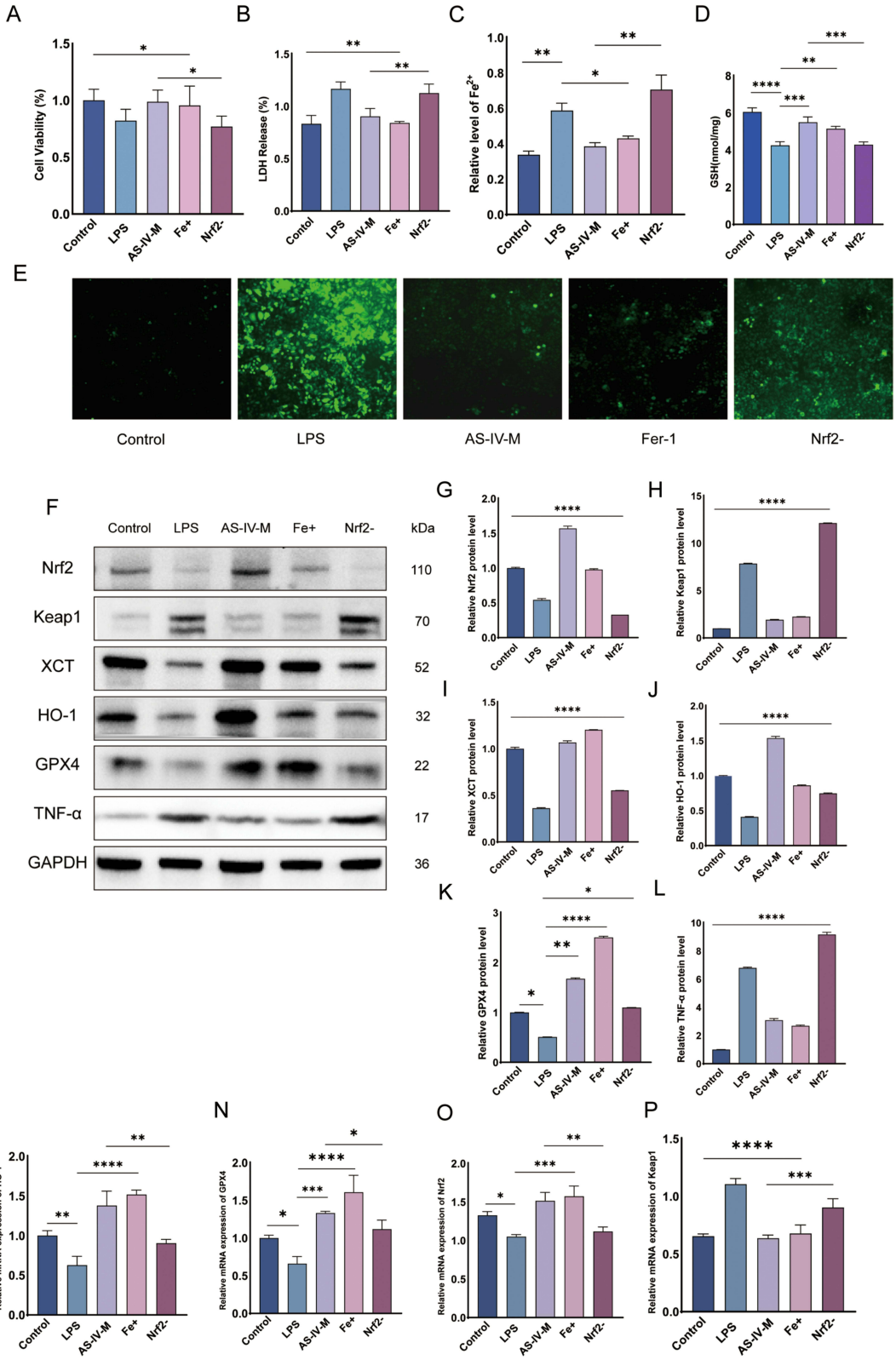

Figure 5 Continued.

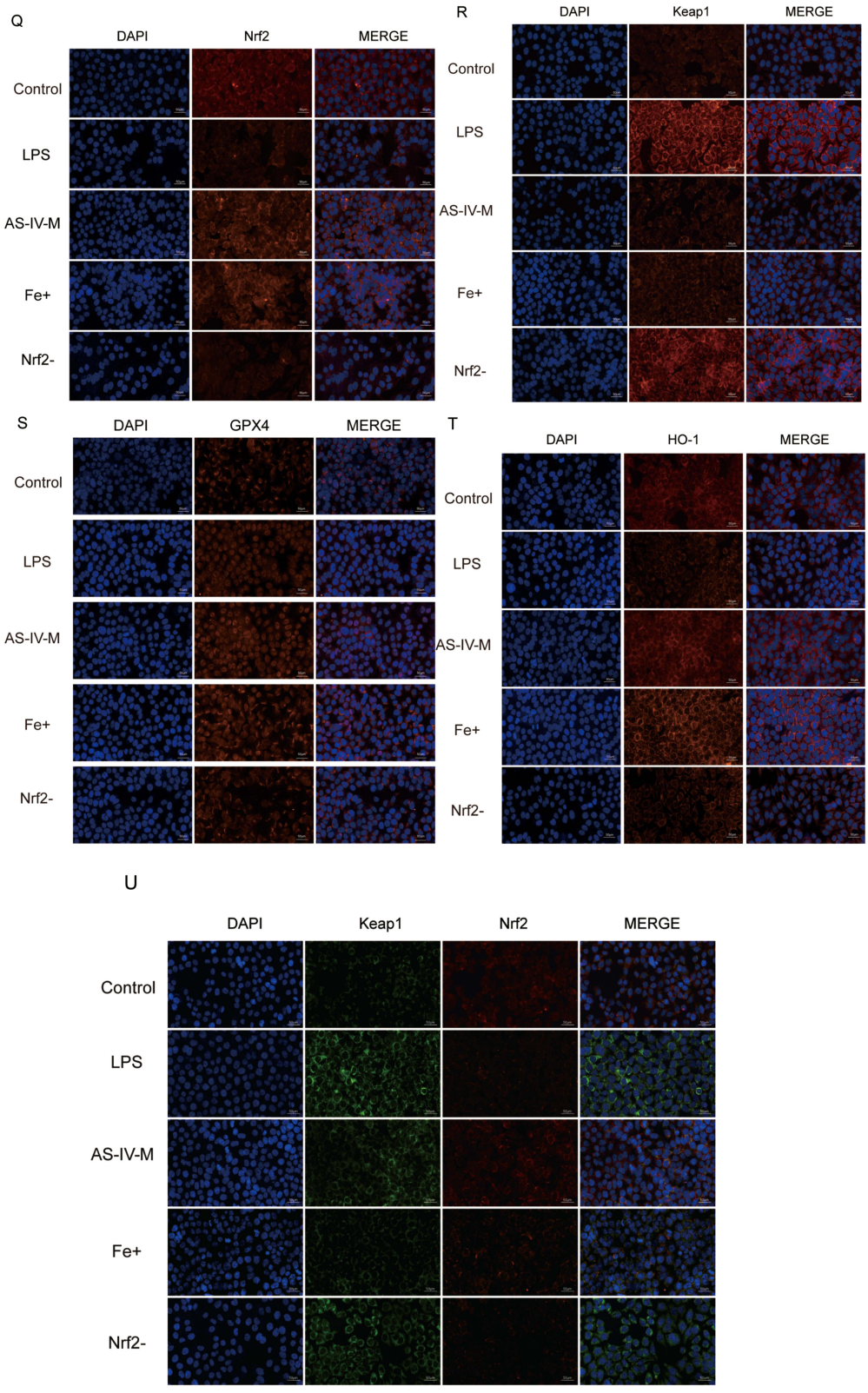

Figure 5 ML385 pretreatment abrogates AS-IV mediated ferroptosis suppression via Nrf2 signaling in RWPE-1 cells. (**A**) Cell viability assessment under combinatorial drug treatments in LPS-stimulated RWPE-1 cells. (**B**–**D**) Biochemical profile analysis: LDH release, iron ion concentration, and GSH content across experimental groups (LPS, AS-IV, ferroptosis inhibitor, ML385+AS-IV). (**E**) Representative fluorescence imaging of intracellular ROS accumulation. (**F**) Western blotting assay to measure the protein levels of Nrf2, Keap1, XCT, HO-1, GPX4 and TNF-α in LPS-induced RWPE-1, AS-VI-treated, ferroptosis inhibitor and Nrf2 inhibitor + medium-dose AS-IV. (**G**–**L**) Quantitative Western blot analysis of ferroptosis-related proteins and inflammatory factors. (**M**–**P**) qRT-PCR analysis of Nrf2 pathway-related gene expression. (**Q**–**T**) Subcellular localization analysis via immunofluorescence staining. (**U**) Co-localization analysis of Keap1-Nrf2 interaction. Data represent mean ± SD. Statistical comparisons performed using one-way ANOVA (**A**–**D** and **G**–**P**). Significance levels: *P<0.05; **P<0.01; ***P<0.001; ****P<0.0001.

https://doi.org/10.2147/JIR.S527722

and reduced reactive oxygen species (ROS) by 72%, confirming its ability to mitigate oxidative stress and enhance antioxidant defenses (Figure 5D and E). AS-IV significantly reduced the intracellular ferrous ion accumulation, effectively suppressed ferroptosis (Figure 5C). Western blot analysis revealed dose-dependent upregulation of Nrf2, HO-1,Cystine/Glutamate Transporter (xCT) and GPX4, along with downregulation of Keap1 and TNF-α. These findings demonstrate that the activation of the Nrf2 pathway enhances antioxidant enzyme activity and mitigates oxidative damage (Figures 5F–L). RT-qPCR validated these observations, showing increased mRNA levels of Nrf2, HO-1, and GPX4 with suppressed Keap1 expression (Figure 5M–P). Immunofluorescence assays confirmed enhanced Nrf2 nuclear translocation and reduced Keap1-Nrf2 colocalization, indicating that AS-IV disrupted Keap1/Nrf2 complex formation to activate antioxidant defenses (Figure 5Q–U). Notably, co-treatment with an Nrf2 inhibitor abolished AS-IV's anti-ferroptotic effects of AS-IV, as evidenced by the persistent lipid peroxidation and unresolved inflammation. Immunofluorescence co-staining revealed reduced nuclear Nrf2 accumulation and enhanced Keap1-Nrf2 co-localization in the inhibitor group, confirming Nrf2's central role in mediating both the antiferromagnetic and anti-inflammatory effects (Figure 5U). In summary, AS-IV suppressed ferroptosis in RWPE-1 cells by activating the Nrf2 pathway, which improved oxidative stress management and enhanced the cytoprotective mechanisms. The essential role of Nrf2 activation in these protective processes highlights AS-IV's therapeutic potential for ferroptosis-associated pathologies, particularly in those involving chronic inflammation.

Molecular Docking Analysis Reveals Astragaloside IV's Binding Targets Within the Keap1/Nrf2 Antioxidant Pathway

We studied the binding modes and interactions between the target protein and AS-IV by molecular docking. As shown in the figure, the proteins were represented in cartoon, and AS-IV was shown in pink sticks. Key residues are displayed as sticks. Through docking, we found that NRF2 (cyan) PHE-83, GLU-82, THR-80, GLU-79, GLU-78, ASN-382, ARG-380, ARG-415, SER-555, TYR-525 on KEAP1 (blue) could form five hydrogen bond interactions (Figure 6A). We then

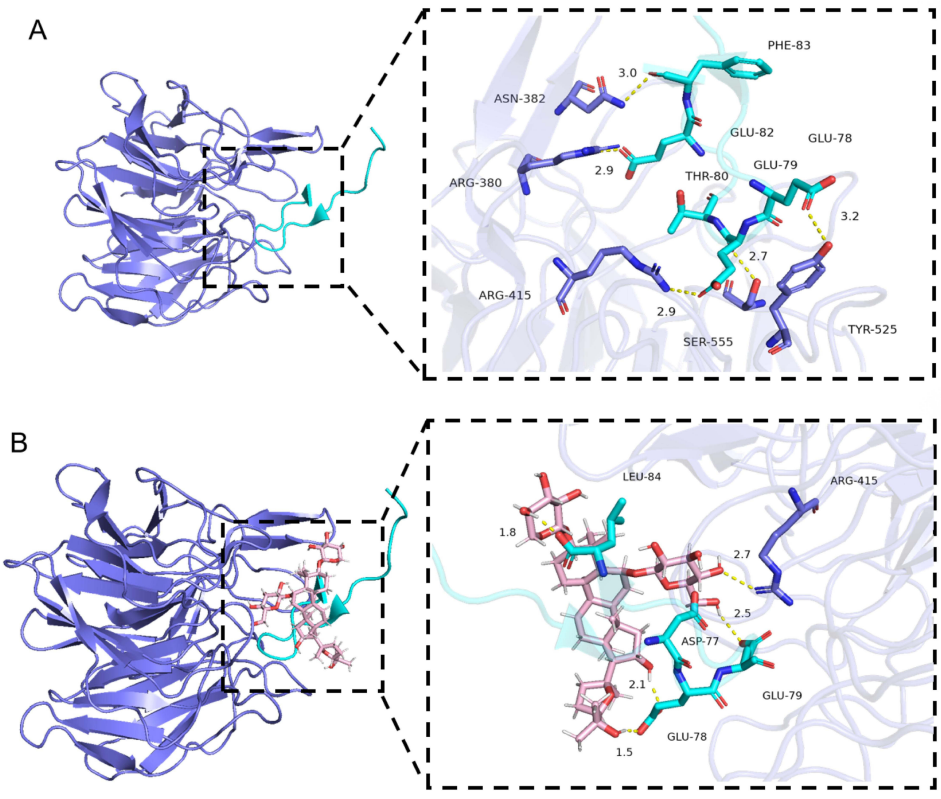

Figure 6 Molecular docking analysis of AS-IV with Keap1 and Nrf2. (**A**) Nrf2 (cyan) PHE-83, GLU-82, THR-80, GLU-79, GLU-78 and ASN-382, ARG-380, ARG-415, SER-555, TYR-525 on Keap1 (blue) could form five hydrogen bond interactions. (**B**) AS-IV could form five hydrogen bonds with LEU-84, ASP-77, GLU-78 and GLU-79 on Nrf2, and one hydrogen bond with ARG-415 on Keap1.

docked to the proteins, and AS-IV formed five hydrogen bonds with LEU-84, ASP-77, GLU-78, and GLU-79 on NRF2 and one hydrogen bond with ARG-415 on KEAP1 (Figure 6B). These interactions are crucial for the stability of proteins and ligands and can significantly affect their biological functions.

Discussion

This study provides the first evidence that AS-IV alleviates CP/CPPS by suppressing ferroptosis through the activation of the Nrf2 antioxidant pathway. AS-IV treatment significantly reduced the levels of ferroptosis markers in prostate tissue, while enhancing antioxidant enzymes. It concurrently suppresses inflammatory cytokines and fibrosis progression.[37,38] Mechanistically, AS-IV promotes Nrf2 nuclear translocation and HO-1 expression, restores glutathione metabolism, and inhibits lipid peroxidation, thereby disrupting the ferroptosis-inflammation cycle.[39]

These findings identify novel therapeutic targets for CP/CPPS and pioneer new approaches for studying programmed cell death regulation by natural compounds.[40] This study provides two key innovations: 1. Mechanistically, ferroptosis has been established as a novel pathological component of CP/CPPS, uncovering the "oxidative stress-ferroptosis-chronic inflammation" axis; 2. Therapeutically, it demonstrated AS-IV multi-target effects through Nrf2 pathway activation, demonstrating the potential of natural compounds for treating inflammatory diseases. AS-IV suppresses ferroptosis by activating the Nrf2 antioxidant pathway.[41] In CP/CPPS models, prostate tissues showed reduced Keap1 protein levels and increased nuclear Nrf2 accumulation, suggesting AS-IV disrupts Keap1-Nrf2 binding to enhance antioxidant responses.[20,42,43] This mechanism further activates downstream antioxidant genes HO-1 and GPX4, enhancing cellular capacity to neutralize lipid peroxidation. Additionally, AS-IV suppresses ferroptosis by downregulating ACSL4 (a pro-ferroptotic regulator) and inhibiting iron overload, which are key drivers of cell death. AS-IV's TNF-α suppression may concurrently inhibit NLRP3 inflammasome assembly, potentially disrupting pyroptosis. Given the crosstalk between ferroptosis (GPX4↓) and pyroptosis (caspase-1↑) via mitochondrial DAMP future studies will delineate this axis. Notably, HO-1 exhibits a dual role: its enzymatic product bilirubin scavenges ROS, whereas AS-IV maintains stable labile iron levels, suggesting selective modulation of HO-1's antioxidant activity to avoid potential pro-ferroptotic effects.

Ferroptosis is mechanistically linked to the CP/CPPS pathology. Evidence indicates that there are three ferroptosis-driven disease progression pathways: 1. Inflammatory Signaling: DAMPs (eg, HMGB1) released during ferroptosis activate TLR4/NF-κB signaling, increasing pro-inflammatory cytokines in prostate tissue; 2. Neuronal Sensitization: Lipid peroxides directly damage the periurethral nerve terminals, inducing mechanical allodynia; 3. Fibrotic Remodeling: Ferroptosis-generated oxidative stress activates fibroblast mechanotransduction pathways, driving abnormal extracellular matrix deposition.[44,45] Compared to conventional medications such as NSAIDs, AS-IV demonstrates unique advantages by targeting both the underlying mechanisms (oxidative stress) and downstream effects (inflammatory amplification) of specific cellular death pathways. At the level of oxidative stress, AS-IV appears to restore intracellular antioxidant defenses by modulating the nucleocytoplasmic shuttling of redox-sensitive transcription factors, thereby effectively rebuilding cellular protection systems. Regarding inflammatory regulation, its mechanisms extend to modifying the membrane localization of damage-sensing receptors, suggesting broader immunomodulatory effects. In contrast, traditional NSAIDs primarily provide symptomatic relief without addressing the pathological cycle, as they mainly inhibit prostaglandin synthesis through COX enzyme blockade.[39,46] Current first-line CP/CPPS therapies (α-blockers and antibiotics) demonstrate limited efficacy in 46% of refractory cases, as their mechanisms focus on smooth muscle modulation and pathogen suppression without addressing the core pathophysiology. AS-IV demonstrates therapeutic efficacy not only through anti-inflammatory effects, but also by fundamentally intervening in pathological processes via modulation of ferroptosis-related pathways.[43] In contrast, synthetic compounds like Ferrostatin-1, while specifically inhibit ferroptosis, lack comprehensive therapeutic capacities such as anti-fibrotic activity and immunomodulation, thereby failing to address the multidimensional symptoms of CP/CPPS. Emerging evidence has revealed that ferroptosis plays a pivotal role in chronic kidney disease and neurodegenerative disorders; however, its involvement in CP/CPPS pathogenesis remains underexplored.[40,47] Groundbreaking studies have identified characteristic ferroptosis markers in CP/CPPS prostate tissues, with AS-IV showing a unique capacity to reverse these alterations through Nrf2 pathway activation.[47] Compared to other herbal components (eg, curcumin and resveratrol), AS-IV exhibits superior selectivity in

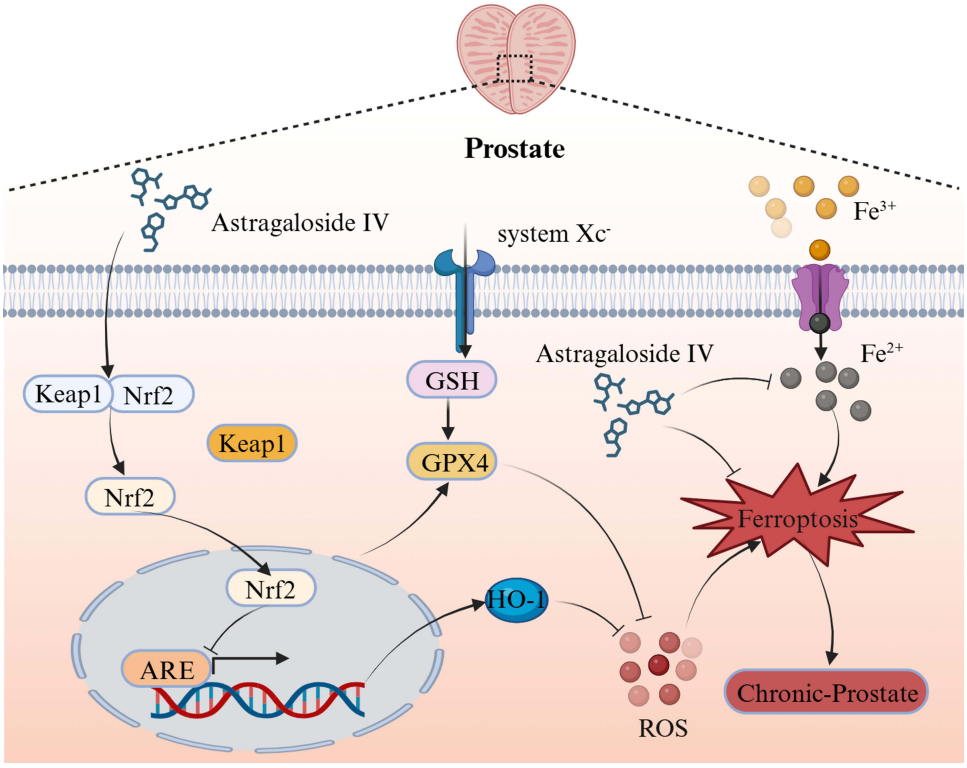

Figure 7 Therapeutic mechanism of Astragaloside IV in experimental autoimmune prostatitis. AS-IV ameliorates chronic prostatitis/chronic pelvic pain syndrome in EAP rats through three core mechanisms:1. Keap1/Nrf2/HO-1 axis activation; 2. Iron homeostasis regulation; 3. Oxidative damage suppression.

HO-1 regulation while avoiding adverse effects associated with free iron accumulation, a critical safety advantage supporting its clinical translation (Figure 7).

This study establishes critical theoretical foundations for the clinical translation of AS-IV, particularly in addressing the current therapeutic limitations of CP/CPPS. Approximately 46% of patients with CP/CPPS exhibit suboptimal responses to conventional therapies (antibiotics and α-blockers), highlighting the need for novel treatment strategies.[48] AS-IV demonstrates unique therapeutic potential by concurrently modulating the pathological interplay between specific cell death pathways and chronic inflammation. As a second-line or adjunctive agent, AS-IV shows synergistic effects when combined with NSAIDs, thereby enhancing the therapeutic outcomes through complementary mechanisms. Although α-blockers alleviate urinary symptoms via urethral smooth muscle relaxation, AS-IV concurrently inhibits prostatic fibrosis and neuroinflammation, targeting fundamental disease progression mechanisms.[49–51] Although oral bioavailability requires optimization, advanced delivery systems (nanoparticle formulations and lipid encapsulation) successfully employed for other herbal compounds could enhance AS-IV's clinical applicability.[52–54]

Although this study elucidates the mechanism by which AS-IV inhibits ferroptosis via the Keap1/Nrf2/HO-1 pathway, several limitations warrant consideration. First, the rat CP/CPPS model exhibits distinct prostate anatomical structures and immune microenvironment characteristics compared with humans. While EAP rats and RWPE-1 cells provide reductionist models for mechanistic dissection, clinical translation requires confronting human tissue complexity**. Future studies with spatially resolved transcriptomics on clinical biopsies will map ferroptosis heterogeneity across prostate niches. Further validation using patient-derived organoids or clinical tissue samples is recommended. Second, although the dosage and treatment duration were based on preliminary studies, a systematic exploration of the optimal therapeutic windows (eg, low-dose long-term vs high-dose short-term regimens) remains necessary. Third, the precise ferroptosis triggers in CP/CPPS (eg, specific pathogen infections or autoantibodies) require clarification. Additionally, crosstalk between the Keap1/Nrf2/HO-1 pathway and other programmed cell death mechanisms (eg, apoptosis and pyroptosis) requires further investigation. Finally, comprehensive multiorgan toxicological assessments are required to

evaluate the potential long-term effects of AS-IV, particularly on reproductive function.Despite compelling mechanistic data, clinical translation requires addressing:Species divergence: Rat prostate stroma dominates (>70% volume) versus human epithelium-centric anatomy. Ongoing patient-derived organoid studies will verify AS-IV efficacy in human tissue contexts; Long-term safety: While AS-IV showed no toxicity at 40 mg/kg over 4 weeks, chronic exposure risks (eg, thyroid dysfunction) warrant Phase I monitoring; Biomarker refinement: Serum MDA/GSH ratios, though informative, lack prostate specificity. Integrating imaging-based redox sensors could improve clinical response assessment. These limitations, however, catalyze future research rather than diminish present findings.

Future research should focus on three key directions. First, multicenter clinical trials should be conducted to evaluate AS-IV's efficacy and safety of AS-IV in CP/CPPS patients, with focused monitoring of pain scores (VAS), NIH-CPSI indices, and radiologic fibrosis regression rates. Second, single-cell RNA sequencing was employed to characterize the heterogeneity in ferroptosis-sensitive cellular subtypes (eg, epithelial cells and fibroblasts) within the prostate microenvironment, while identifying AS-IV's specific molecular targets of AS-IV. Third, combination therapies with other ferroptosis inhibitors (eg, Liproxstatin-1) or antifibrotic agents (eg, pirfenidone) can enhance the therapeutic efficacy through synergistic effects. Additionally, investigating the generalizability of ferroptosis mechanisms across chronic pelvic pain syndromes (eg, interstitial cystitis) could expand AS-IV's clinical applications of AS-IV.

Conclusion

This study is the first to demonstrate that AS-IV alleviates CP/CPPS progression by suppressing ferroptosis through Keap1/Nrf2/HO-1 pathway activation, effectively mitigating inflammatory responses, oxidative stress, and fibrotic remodeling. These findings not only identify novel therapeutic targets for CP/CPPS management, but also establish a paradigm for investigating programmed cell death regulation by botanical monomers in traditional Chinese medicine. Clinically, the multitarget properties and favorable safety profile of the AS-IV position are promising candidates for refractory CP/CPPS. Future research should focus on drug formulation optimization and combination therapy strategies, which may enable AS-IV to play an expanded role in the precise management of chronic inflammatory disorders.

Abbreviations

CP/CPPS, Chronic prostatitis/chronic pelvic pain syndrome; astragaloside IV, the primary bioactive component of Astragalus membranaceus; CFA, Complete Freund's adjuvant; RWPE-1, human prostatic epithelial cell; LPS, lipopolysaccharide; MDA, malondialdehyde; GSH, glutathione; GPX4, glutathione peroxidase 4; HO-1, heme oxygenase-1; TNF-α, tumor necrosis factor-alpha; IL-6, interleukin-6; xCT, Cystine/Glutamate Transporter; FTH1 (Ferritin Heavy Chain 1) DAMP, damage-associated molecular pattern; ARE, antioxidant response elements; TCM, traditional Chinese medicine; CFA, complete Freund's Adjuvant; EAP, experimental autoimmune prostatitis; H&E, Hematoxylin and eosin; SOD, Superoxide dismutase; ROS, reactive oxygen species.

Data Sharing Statement

Data used to support the findings of this study are available from the corresponding author upon request.

Ethics Approval and Informed Consent

All animal procedures were approved by the Committee for Animal Care and Use of the Animal Center of Zhejiang Chinese Medical University, in accordance with the Chinese guidelines for welfare and ethics for laboratory animals (Approval No. IACUC-20221024-05).

Consent to Publication

All authors agree to the publication of this work.

Funding

This work and related studies were supported by the Natural Science Foundation of Zhejiang Province (grant No. LY20H270003) and Zhejiang Traditional Chinese Medicine Administration (grant No. 2022ZZ017).

Disclosure

The authors have declared that no competing interest exists for this work.

References

1. Ye ZQ, Zeng XY. Advances in the diagnosis and treatment of chronic prostatitis. *Natl J Androl*. 2003;9(7):483–488.
2. Hua-Wei L, Xiao-Bo D. Prostant combined with α-blockers versus single Prostant for type III prostatitis: a meta-analysis. *J Urol*. 2017;2017:1.
3. Chen J, Zhang J, Chen T, et al. Xiaojianzhong decoction attenuates gastric mucosal injury by activating the p62/Keap1/Nrf2 signaling pathway to inhibit ferroptosis. *Biomed Pharmacother*. 2022;155:113631. doi:10.1016/j.biopha.2022.113631
4. Song WJ, Liu XY, He LYJF, Microbiology I. Research progress on the relationship between chronic prostatitis/chronic pelvic pain syndrome and the microbiota of the reproductive system. *Frontiers in Cellular and Infection Microbiology*. 2024;14. doi:10.3389/fcimb.2024.1417276
5. Jia Z, Lv D, Chen T, et al. Network pharmacology and in vivo experiment-based strategy for investigating the mechanism of chronic prostatitis/chronic pelvic pain syndrome in QianLieJinDan tablets. Article. *Heliyon*. 2024;10(9):e29975. doi:10.1016/j.heliyon.2024.e29975
6. Lin DX, Zhang MY, Luo CC, Wei PY, Cui K, Chen Z. Targeting Ferroptosis Attenuates Inflammation, Fibrosis, and Mast Cell Activation in Chronic Prostatitis. *J Immunol Res*. 2022;20226833867. doi:10.1155/2022/6833867
7. Yang J, Luan JC, Chen JH, et al. Prostate-derived IL-1β upregulates expression of NMDA receptor in the paraventricular nucleus and shortens ejaculation latency in rats with experimental autoimmune prostatitis. *Asian J Androl*. 2022;24(2):213. doi:10.4103/aja202142
8. Mu K, Yang Y, An X, et al. Proteomic analysis of urinary exosomes reveals ferroptosis-associated proteins are involved in diabetic nephropathy. *Genes Dis*. 2024;11(5):101138. doi:10.1016/j.gendis.2023.101138
9. Kensler TW, Wakabayashi N, Biswal S. Cell survival responses to environmental stresses via the Keap1-Nrf2-ARE pathway. Research Support, N.I.H. Extramural; Research Support, Non-U.S. Government; Review. *Annu Rev Pharmacol Toxicol*. 2007;47(1):89–116. doi:10.1146/annurev.pharmtox.46.120604.141046
10. Mulens-Arias V, Manuel Rojas J, Barber DF. The Intrinsic Biological Identities of Iron Oxide Nanoparticles and Their Coatings: unexplored Territory for Combinatorial Therapies. Review. *Nanomaterials*. 2020;10(5):837. doi:10.3390/nano10050837
11. Ren S, Zhang H, Mu Y, Sun M, Liu P. Pharmacological effects of Astragaloside IV: a literature review: review. *J Traditional Chin Med*. 2013;33(3):413–416. doi:10.1016/s0254-6272(13)60189-2
12. Wan J, Zhang Z, Wu C. Astragaloside IV derivative HHQ16 ameliorates infarction-induced hypertrophy and heart failure through degradation of lncRNA4012/9456. *Signal Transduct Targeted Ther*. 2023;8(1):414.
13. Leng B, Zhang Y, Liu X, et al. Astragaloside IV Suppresses High Glucose-Induced NLRP3 Inflammasome Activation by Inhibiting TLR4/NF-κB and CaSR. Article. *Mediators Inflammation*. 2019;2019:20191082497. doi:10.1155/2019/1082497
14. Lu M, Tang F, Zhang J, et al. Astragaloside IV Attenuates Injury Caused by Myocardial Ischemia/Reperfusion in Rats via Regulation of Toll-Like Receptor 4/Nuclear Factor-κB Signaling Pathway: article. *Phytother Res*. 2015;29(4):599–606. doi:10.1002/ptr.5297
15. Tuerxun D, Aierken R, Zhang Y-M, et al. Astragaloside IV alleviates lipopolysaccharide-induced preeclampsia-like phenotypes via suppressing the inflammatory responses. *Kaohsiung J Med Sci*. 2021;37(3):236–244. doi:10.1002/kjm2.12313
16. Xu W, Shao X, Tian L, et al. Astragaloside IV ameliorates renal fibrosis via the inhibition of mitogen-activated protein kinases and antiapoptosis in vivo and in vitro: review. *J Pharmacol Exp Ther*. 2014;350(3):552–562. doi:10.1124/jpet.114.214205
17. Luo L-F, Qin L-Y, Wang J-X, Guan P, Wang N, Ji E-S. Astragaloside IV Attenuates the Myocardial Injury Caused by Adriamycin by Inhibiting Autophagy. *Front Pharmacol*. 2021;12669782. doi:10.3389/fphar.2021.669782
18. Jin H, Jiao Y, Guo L, et al. Astragaloside IV blocks monocrotaline-induced pulmonary arterial hypertension by improving inflammation and pulmonary artery remodeling. Article. *IntJ Mol Med*. 2021;47(2):595–606. doi:10.3892/ijmm.2020.4813
19. Qin S, Yin J, Huang S, et al. Astragaloside IV Protects Ethanol-Induced Gastric Mucosal Injury by Preventing Mitochondrial Oxidative Stress and the Activation of Mitochondrial Pathway Apoptosis in Rats. *Front Pharmacol*. 2019:10894. doi:10.3389/fphar.2019.00894.
20. Liu Z, Zhou Z, Ai P, Zhang C, Chen J, Wang Y. Astragaloside IV attenuates ferroptosis after subarachnoid hemorrhage via Nrf2/HO-1 signaling pathway. *Front Pharmacol*. 2022;13924826. doi:10.3389/fphar.2022.924826
21. Chiang S-K, Chen S-E, Chang L-C. A Dual Role of Heme Oxygenase-1 in Cancer Cells. Review. *Int J Mol Sci*. 2019;20(1):39. doi:10.3390/ijms20010039
22. Jiang Z, Yang H, Ni W, et al. Attenuation of neuronal ferroptosis in intracerebral hemorrhage by inhibiting HDAC1/2: microglial heterogenization via the Nrf2/HO1 pathway. *CNS Neurosci Ther*. 2024;30(3):e14646. doi:10.1111/cns.14646
23. Qian Z, Zhang Q, Li P, Yang Z, Yanan L, Rulin Z. A Disintegrin and Metalloproteinase-8 Protects Against Erastin-Induced Neuronal Ferroptosis via Activating Nrf2/HO-1/FTH1 Signaling Pathway. *J Mol Neurobiol*. 2024;61(6):3490–3502. doi:10.1007/s12035-023-03782-1
24. Hua XL, Ge SD, Zhang M, et al. Pathogenic Roles of CXCL10 in Experimental Autoimmune Prostatitis by Modulating Macrophage Chemotaxis and Cytokine Secretion. *Front Immunol*. 2021:12706027. doi:10.3389/fimmu.2021.706027.
25. Zhang J, Chen J, Jiang Q, et al. Resolvin D1 Attenuates Inflammation and Pelvic Pain Associated with EAP by Inhibiting Oxidative Stress and NLRP3 Inflammasome Activation via the Nrf2/HO-1 Pathway. *J Inflamm Res*. 2023;16:3365–3379. doi:10.2147/jir.S408111
26. Wang X, Wang Y, Huang D, et al. Astragaloside IV regulates the ferroptosis signaling pathway via the Nrf2/SLC7A11/GPX4 axis to inhibit PM2.5-mediated lung injury in mice. *Int Immunopharmacol*. 2022;112:109186. doi:10.1016/j.intimp.2022.109186
27. Magro F, Sabino J, Rosini F, et al. ECCO Position on Harmonisation of Crohn's Disease Mucosal Histopathology. *J Crohns Colitis*. 2022;16(6):876–883. doi:10.1093/ecco-jcc/jjac006
28. Li C, Liu M, Deng L, Luo D, Ma R, Lu Q. Oxyberberine ameliorates TNBS-induced colitis in rats through suppressing inflammation and oxidative stress via Keap1/Nrf2/NF-xB signaling pathways. *Phytomedicine*. 2023;116:154899. doi:10.1016/j.phymed.2023.154899
29. Wei L-F, Zhang H-M, Wang -S-S, et al. Changes of MDA and SOD in Brain Tissue after Secondary Brain Injury with Seawater Immersion in Rats. *Turk Neurosurg*. 2016;26(3):384–388. doi:10.5137/1019-5149.Jtn.8265-13.1
30. Liu YF, Xie WJ, Xi P, et al. Astaxanthin alleviates chronic prostatitis/chronic pelvic pain syndrome by increasing colonization of Akkermansia muciniphila in the intestine. *Phytomedicine*. 2024;123:155249. doi:10.1016/j.phymed.2023.155249

31. Xiao S, Zhou T, Pan J, et al. Identifying autophagy-related genes as potential targets for immunotherapy in tuberculosis. *Int Immunopharmacol*. 2023;118:109956. doi:10.1016/j.intimp.2023.109956
32. Suzen S, Tucci P, Profumo E, Buttari B, Saso L. A Pivotal Role of Nrf2 in Neurodegenerative Disorders: a New Way for Therapeutic Strategies. Review. *Pharmaceuticals*. 2022;15(6):692. doi:10.3390/ph15060692
33. Zeng J, Zhao N, Yang J, et al. Puerarin Induces Molecular Details of Ferroptosis-Associated Anti-Inflammatory on RAW264.7 Macrophages. Article. *Metabolites*. 2022;12(7):653. doi:10.3390/metabo12070653
34. Ge C, Peng Y, Li J, et al. Hydroxysafflor Yellow A Alleviates Acute Myocardial Ischemia/Reperfusion Injury in Mice by Inhibiting Ferroptosis via the Activation of the HIF-1α/SLC7A11/GPX4 Signaling Pathway. *Nutrients*. 2023;15(15):3411. doi:10.3390/nu15153411
35. Guo X, Hao Y, Ma H, et al. The mechanism of monobutyl phthalate-induced ferroptosis via TNF/IL6/STAT3 signal pathway in TM-3 cells. Article. *J Toxicological Sci*. 2023;48(5):299–310. doi:10.2131/jts.48.299
36. Feng J, Zhou S, Xie Q, et al. Traditional Chinese medicine shenhuang granule in patients with severe/critical COVID-19: a randomized controlled multicenter trial. *Phytomedicine*. 2021;89:153612. doi:10.1016/j.phymed.2021.153612
37. Li L, Huang W, Wang S, et al. Astragaloside IV Attenuates Acetaminophen-Induced Liver Injuries in Mice by Activating the Nrf2 Signaling Pathway. Article. *Molecules*. 2018;23(8):2032. doi:10.3390/molecules23082032
38. Zhang C, Shi Z, Xu Q, et al. Astragaloside IV alleviates stroke-triggered early brain injury by modulating neuroinflammation and ferroptosis via the Nrf2/HO-1 signaling pathway. *Acta Cir Bras*. 2023;38(1):e380723. doi:10.1590/acb380723
39. Zheng T, Jiang T, Huang Z, Ma H, Wang M. Role of traditional Chinese medicine monomers in cerebral ischemia/reperfusion injury: a review of the mechanism. Review. *Front Pharmacol*. 2023;14:1220862. doi:10.3389/fphar.2023.1220862
40. Su Y, Xu J, Chen S, et al. Astragaloside IV protects against ischemia/reperfusion (I/R)-induced kidney injury based on the Keap1-Nrf2/ARE signaling pathway. *Transl Androlo Urol*. 2022;11(8):1177–1188. doi:10.21037/tau-22-505
41. Wu X, Wei J, Yi Y, Gong Q, Gao J. Activation of Nrf2 signaling: a key molecular mechanism of protection against cardiovascular diseases by natural products. Review. *Front Pharmacol*. 2022;13:1057918. doi:10.3389/fphar.2022.1057918
42. Ding C, Wu Y, Zhan C, et al. Research progress on the role and inhibitors of Keap1 signaling pathway in inflammation. Review. *Int Immunopharmacol*. 2024;141:112853. doi:10.1016/j.intimp.2024.112853
43. Hou K, Liu L, Fang Z-H, et al. The role of ferroptosis in cardio-oncology. Review. *Arch Toxicol*. 2024;98(3):709–734. doi:10.1007/s00204-023-03665-3
44. Fitzgerald KA, Rowe DC, Barnes BJ, et al. LPS-TLR4 signaling to IRF-3/7 and NF-κB involves the toll adapters TRAM and TRIF. Research Support. *J Exp Med*. 2003;198(7):1043–1055. doi:10.1084/jem.20031023
45. Nyati KK, Masuda K, Mahabub-Uz Zaman M, et al. TLR4-induced NF-κB and MAPK signaling regulate the IL-6 mRNA stabilizing protein Arid5a. *Nucleic Acids Res*. 2017;45(5):2687–2703. doi:10.1093/nar/gkx064
46. Zhou Z, Yu Y, Miao J, et al. Research Progress of Traditional Chinese Medicine in Treating Central Nervous System Diseases by Modulating Ferroptosis. Article. *Am J Chin Med*. 2024;52(07):1989–2019. doi:10.1142/s0192415x24500770
47. Chai Z, Zheng J, Shen J. Mechanism of ferroptosis regulating ischemic stroke and pharmacologically inhibiting ferroptosis in treatment of ischemic stroke: review. *CNS Neurosci Ther*. 2024;30(7):e14865. doi:10.1111/cns.14865
48. Polackwich AS, Shoskes DA. Chronic prostatitis/chronic pelvic pain syndrome: a review of evaluation and therapy. *Prostate Cancer and Prostatic Diseases*. 2016;19(2):132–138. doi:10.1038/pcan.2016.8
49. Chen H, Hoi MPM, Lee SMY. Medicinal plants and natural products for treating overactive bladder. Review. *ChinMed*. 2024;19(1):56. doi:10.1186/s13020-024-00884-3
50. Leisegang K, Henkel R, Agarwal A. Obesity and metabolic syndrome associated with systemic inflammation and the impact on the male reproductive system. Review. *Am J Reprod Immunol*. 2019;82(5):e13178. doi:10.1111/aji.13178
51. Zhong J, Tan L, Chen M, He C. Pharmacological activities and molecular mechanisms of Pulsatilla saponins. Review. *ChinMed*. 2022;17(1):59. doi:10.1186/s13020-022-00613-8
52. Talebian S, Wallace GG, Schroeder A, Stellacci F, Conde J. Nanotechnology-based disinfectants and sensors for SARS-CoV-2. Article. *Nature Nanotechnol*. 2020;15(8):618–621. doi:10.1038/s41565-020-0751-0
53. Wang J, Wu X, Chen J, Gao T, Zhang Y, Yu N. Traditional Chinese medicine polysaccharide in nano-drug delivery systems: current progress and future perspectives. Review. *Biomed Pharmacother*. 2024;173:116330. doi:10.1016/j.biopha.2024.116330
54. Kong C, Sun J, Hu X, Li G, Wu S. A tumor targeted nano micelle carrying astragaloside IV for combination treatment of bladder cancer. *Sci Rep*. 2024;14(1):17704. doi:10.1038/s41598-024-66010-3